Title

The Role of Structural and Compositional Heterogeneities in the Insulator-to-Metal Transition in Hole-Doped APd_3O_4 (A = Ca, Sr)

Journal

Inorganic Chemistry, 56(9)

ISSN

0020-1669 1520-510X

Authors

Lamontagne, Leo K
Laurita, Geneva
Knight, Michael
et al.

Publication Date

2017-04-13

DOI

10.1021/acs.inorgchem.7b00307

Peer reviewed

The Role of Structural and Compositional Heterogeneities in the Insulator-to-Metal Transition in Hole-Doped APd$_3$O$_4$ (A = Ca, Sr)

Leo K. Lamontagne,[†,‡] Geneva Laurita,[‡] Michael Knight,[‡] Huma Yusuf,[‡] Jerry Hu,[‡] Ram Seshadri,[*,‡,†,¶] and Katharine Page[§]

[†]*Materials Department, University of California, Santa Barbara, California 93106, United States*

[‡]*Materials Research Laboratory, University of California, Santa Barbara, California 93106, United States*

[¶]*Department of Chemistry and Biochemistry, University of California, Santa Barbara, California 93106, United States*

[§]*Chemical and Engineering Materials Division, Spallation Neutron Source Oak Ridge National Laboratory, Oak Ridge, Tennessee 37831, United States*

E-mail: seshadri@mrl.ucsb.edu

Abstract

The cubic semiconducting compounds APd$_3$O$_4$ (A = Ca, Sr) can be hole-doped by Na substitution on the A site and driven towards more conducting states. This process has been followed here by a number of experimental techniques in order to understand the evolution of electronic properties. While an insulator-to-metal transition is observed in Ca$_{1-x}$Na$_x$Pd$_3$O$_4$ for $x \geq 0.15$, bulk metallic behavior is not observed for Sr$_{1-x}$Na$_x$Pd$_3$O$_4$ up to $x = 0.20$. Given the very similar crystal and (calculated) electronic structures of the two materials, the distinct behavior is a matter of interest. We present evidence of local disorder in the A = Sr materials through the analysis of the neutron pair distribution function which is potentially at the heart of the distinct behavior. Solid-state ^{23}Na nuclear magnetic resonance studies additionally suggest a percolative insulator-to-metal transition mechanism wherein presumably small regions with a signal resembling metallic NaPd$_3$O$_4$ form almost immediately upon Na substitution, and this signal grows monotonically with substitution. Some signatures of increased local disorder and a propensity for Na clustering are seen in the A = Sr compounds.

Introduction

The study of insulator-to-metal transitions is an important topic in the fields of materials chemistry and condensed-matter physics. The profound change in properties associated with the transition are of great fundamental interest, even at the level of separating the elements into metals and non-metals.[1] In addition, a huge range of useful materials functionalities are often found associated with materials that display such transitions.[2,3] In particular, understanding compositionally driven insulator-to-metal transitions in which carriers are doped into a material can lead to tuned carrier concentrations for optimal electrical properties in thermoelectric materials[4] or elevated T_c in superconductors.[5] An important question regarding the nature of the transition driven by charge carrier dop-

ing into semiconducting or insulating hosts is whether the transition is percolative (in the sense of forming as puddles of metal in the insulating background that coalesce at some concentration and drive the entire system metallic), or whether it occurs suddenly across the entirety of the material. Percolation of metallic regions is believed to lead to the colossal magnetoresistance observed in $LaMnO_3$,[6–8] and leads to interesting magnetic and electronic properties in Sr substituted $La_{1-x}Sr_xCoO_3$.[9–12] While the change in carrier concentration can be estimated based on the amount of doping, there are other considerations that can affect the onset of an insulator-to-metal transition. The size of the dopant ion relative to the crystallographic site, as well as complimentary changes in valence to maintain neutrality can impart local distortions that can also affect an insulator-to-metal transition.[13]

Many complex palladium oxides have been previously shown to undergo compositional insulator-to-metal transitions.[14–18] The small bandgaps and significant Pd-d states just below the Fermi level in complex palladium oxides allows for the ease of hole-doping. Previous studies have suggested that some palladium oxides may have unique gapless electronic structures that can lead to interesting physics,[19,20] though these results may be influenced by the tendency of some DFT functionals to underestimate bandgaps in small bandgap semiconductors.[21] Furthermore, complex palladium oxides are typically diamagnetic, allowing for more detailed studies of local structural changes throughout insulator-to-metal transitions with the use of solid-state NMR, which, while useful in examining local phase separation, is difficult to utilize in magnetic oxide materials.[22,23] Recently, we have observed a high Seebeck coefficient with metallic conductivity in the complex palladium oxide $PbPdO_2$ when it undergoes an insulator-to-metal transition with Li-substitution.[24] A better understanding of the insulator-to-metal transitions can lead to improvements in the functional properties of these and other oxide materials.

$CaPd_3O_4$ and $SrPd_3O_4$ both crystallize in the cubic $NaPt_3O_4$ structure type, highlighted in Figure 1. The alkaline-earth cation resides in an 8-coordinate cubic site, while the d^8

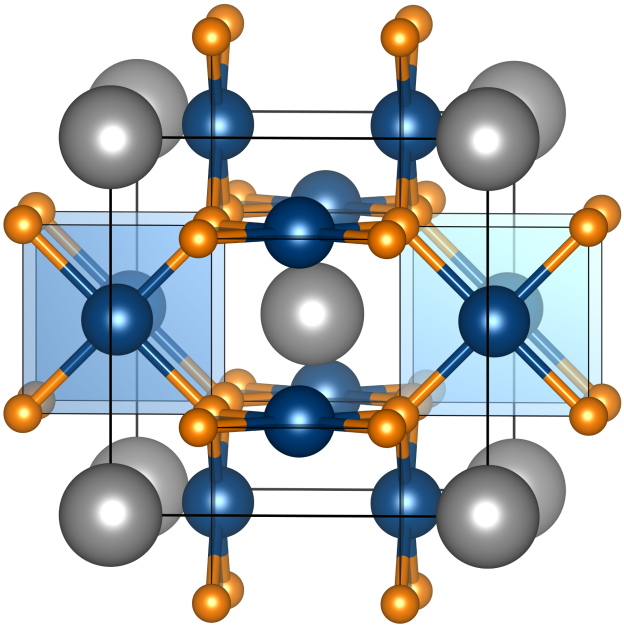

Figure 1: Crystal structure of APd$_3$O$_4$ (A = Ca, Sr) in cubic $Pm\bar{3}n$ (#74). Ca/Sr, Pd, and O are colored silver, blue, and orange respectively. The PdO$_4$ square planes in APd$_3$O$_4$ exhibit 3D corner connectivity. The alkaline-earth element sits in a symmetric, 8-coordinate, cubic site. The Wyckoff positions are A in 2a (0, 0, 0,); Pd in 6c ($\frac{1}{4}$, 0, $\frac{1}{2}$); and O in 8e ($\frac{1}{4}$, $\frac{1}{4}$,$\frac{1}{4}$).

palladium is in its preferred square-planar coordination. The palladium square planes are corner-connected and form a 3D network throughout the crystal.[25] Given the identical crystal structures, one would expect that a compositionally driven insulator-to-metal transition in both CaPd$_3$O$_4$ and SrPd$_3$O$_4$ would occur around the same dopant level assuming the electronic structures were also similar. However, insulator-to-metal transitions in these compounds have been reported to occur under a wide range of hole-dopant levels. Ichikawa and co-workers reported a transition in CaPd$_3$O$_4$ around 10 mol % Li doping onto the Ca site.[16] However, when Na was used as a dopant, Itoh, Yano and Tsuda reported 30 mol % was necessary to drive the transition and remarked how processing can affect the observed electronic properties.[17,26] In the system Sr$_{1-x}$Na$_x$Pd$_3$O$_4$, Taniguchi and co-workers reported a transition around 10 mol % Na.[18]

To better understand the nature of the insulator-to-metal transitions in these compounds and account for the reported differences, we have prepared and processed Ca$_{1-x}$Na$_x$Pd$_3$O$_4$ and Sr$_{1-x}$Na$_x$Pd$_3$O$_4$ with $0 \leq x \leq 0.2$ under identical conditions. The

metallic end-member compound $NaPd_3O_4$ has also been prepared and studied as a reference. We find that while the electronic structures of $CaPd_3O_4$ and $SrPd_3O_4$ are nearly identical, $CaPd_3O_4$ is driven metallic above 10 mol % Na substitution, while $SrPd_3O_4$ remains a semiconductor with a negative $d\rho/dT$ (slope of resistivity as a function of temperature) up to 20 mol % Na substitution. X-ray diffraction studies suggests Na clustering or a distribution gradient in both compounds at high doping levels and, along with solid-state ^{23}Na NMR, suggests a percolative insulator-to-metal transition in $CaPd_3O_4$. However, increased local disorder observed in both NMR and analysis of total scattering data using the pair distribution function suggest disorder as a barrier to bulk metallicity in $SrPd_3O_4$.

Experimental and Computational Methods

Polycrystalline samples of $A_{1-x}Na_xPd_3O_4$ (A = Ca, Sr), $0 \leq x \leq 0.2$, were prepared by heating stoichiometric amounts of $CaCO_3$, $SrCO_3$, PdO, and Na_2CO_3 powders. The precursors were ground in an agate mortar and pestle and pressed into a pellet at 100 MPa. The pellets were placed onto beds of powder of the same composition to prevent contamination from the alumina crucible. The samples were heated at 600 °C for 12 hours in a flowing O_2 tube furnace. This procedure was repeated twice to ensure a complete reaction of the precursors. The end-member $NaPd_3O_4$ was prepared in a similar manner at 700 °C.

The crystal structures were characterized by X-ray powder diffraction on a Panalytical Empyrean powder diffractometer with Cu-K_α radiation. Lattice parameters were determined by mixing the prepared materials with a silicon standard and recording from 10° 2θ to 120° 2θ. The x = 0.05 and x = 0.20 samples were additionally studied through synchrotron X-ray diffraction at the 11-BM beam line at the Advanced Photon Source at Argonne National Laboratory with wavelength $\lambda = 0.414159$ Å. Rietveld[27] refinement was performed using the TOPAS academic software.[28] Crystal structures were visualized using VESTA.[29] Neutron scattering data for pair distribution function (PDF) analysis was

collected at the NOMAD diffractometer[30] at the Spallation Neutron Source, Oak Ridge National Laboratory. Least-squares refinement of the reduced PDF was performed using the PDFgui program.[31] Single pulse ^{23}Na solid-state magic angle spinning (MAS) NMR experiments were performed at 300 K on a Bruker ASCEND III HD 400 MHz (9.4 T) spectrometer. Samples were packed into a 4 mm zirconia rotor with Kel-F caps and spun at a rate of 8 kHz. The single pulse experiment used a pulse length of 0.83 μs corresponding to a $\pi/12$ tip angle. The ^{23}Na shifts were referenced to 1 M NaCl. For electrical resistivity measurements, the materials were sintered as bar pellets approximately 9 mm in length and four copper wires were attached with a silver paste before running them in a He refrigerator from 300 K to 25 K. The electronic structure was calculated using density functional theory (DFT) as implemented in the Vienna *ab initio* Simulation Package (VASP)[32,33] with projector-augmented wave (PAW) pseudopotentials.[34] For structure optimization, the exchange-correlation was described by Perdew-Burke-Ernzerhof within the generalized gradient approximation (GGA-PBE)[35] using a Γ center k-mesh of $8\times8\times8$ and a tetrahedron smearing method. A screened hybrid functional (HSE06)[36] was used to calculate the density of states (DOS).

Results and discussion

Average Structure from Diffraction

Polycrystalline samples of APd$_3$O$_4$ (A = Ca, Sr) were prepared phase pure with up to 20 mol % Na substitution onto the A site. The reactions were done in a flowing O_2 atmosphere at 600 °C to prevent the reduction of the PdO to Pd metal. Rietveld refinements of synchrotron XRD data confirmed the phase purity, shown in Figure 2 for the highest Na substitution levels.

The lattice parameters for the samples were determined through Rietveld refinement of laboratory Cu Kα radiation with a Si standard. The lattice parameters for both the

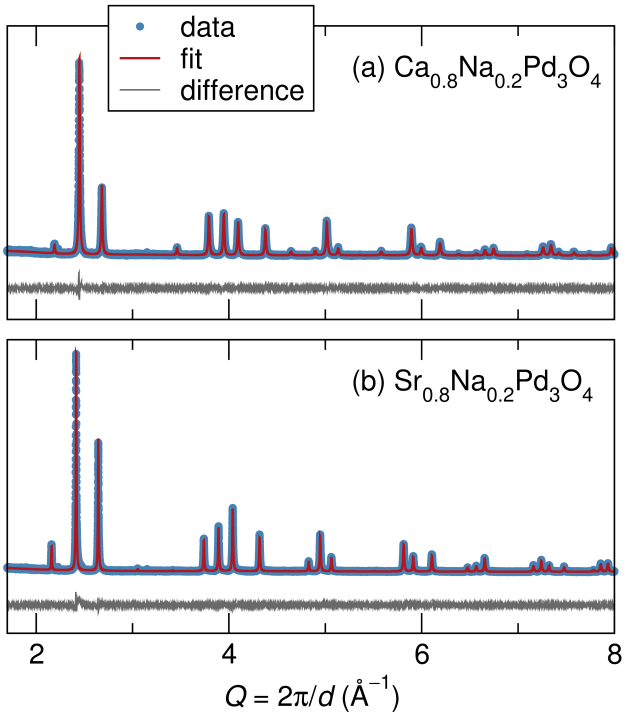

Figure 2: Single phase refinements of nominal (a) $Ca_{0.8}Na_{0.2}Pd_3O_4$ and (b) $Sr_{0.8}Na_{0.2}Pd_3O_4$ from synchrotron X-ray data.

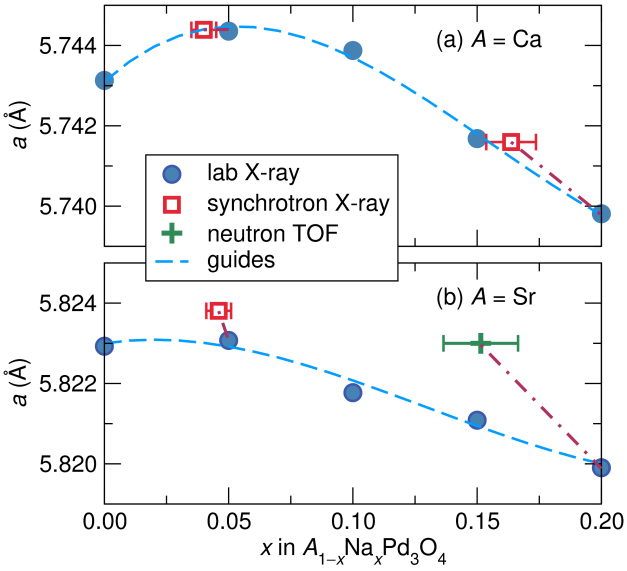

Figure 3: Changes in lattice parameters for (a) $Ca_{1-x}Na_xPd_3O_4$ and (b) $Sr_{1-x}Na_xPd_3O_4$ with Na substitution. Blue circles represent stoichiometric Na substitution levels and lattice parameters refined on a laboratory Cu-K_α diffractometer with a Si standard. Red squares represent refined Na occupancy values and lattice parameters from synchrotron X-ray diffraction data for the nominal $x = 0.05$ and $x = 0.20$ substitution levels. The green plus represents the refined Na occupancy value and lattice parameter using neutron diffraction data.

Ca and Sr materials generally decrease with increasing Na doping, as shown in Figure 3. The lattice parameter for $CaPd_3O_4$ decreases from 5.743 Å to 5.740 Å and the lattice parameter of $SrPd_3O_4$ decreases by an identical amount, from 5.823 Å to 5.820 Å. This is surprising as the ionic radii of Na^{1+} in an 8-coordinate site (1.18 Å) is slightly larger than Ca^{2+} (1.12 Å) and smaller than Sr^{2+} (1.26 Å).[37] This suggests that the decreasing lattice parameter does not primarily arise from the size difference of the dopant ion, but by the necessary oxidation of the Pd^{2+} to Pd^{3+} to maintain charge neutrality. The slight increase in the lattice parameter with small Na substitution in $CaPd_3O_4$ may be attributed to the larger ionic size of the Na^{1+} ion dominating at smaller substitution levels. Refined Na occupancy values and lattice parameters from the synchrotron X-ray data are shown in Figure 3. For the nominal x = 0.05 substitution level, the refined Na occupancies are in good agreement with expectations. Peak tails, which are only seen in the high resolution synchrotron X-ray diffraction data for the x = 0.20 materials lead to an underestimation of the Na occupancy and a slight discrepancy in the refined lattice parameters, the details of which will be discussed presently. Refined values from neutron time of flight (TOF) diffraction data are used in Figure 3 for the x = 0.20 Sr sample as the significant peak tails in the X-ray data prevented reliable refinements.

Electrical Properties and Electronic Structure

In order to study the insulator-to-metal transitions in these materials, the electrical resistivity was measured with successive doping. Pristine $CaPd_3O_4$ displays semiconducting behavior with a room temperature resistivity of 0.1 Ω cm. An insulator-to-metal transition occurs beyond 10 % Na doping as seen through the positive $d\rho/dT$ for the x = 0.15 and x = 0.20 compositions, similar to the substitution amount Ichikawa and co-workers reported upon Li doping in $CaPd_3O_4$.[16] Unsubstituted $SrPd_3O_4$ exhibits a room temperature resistivity almost identical to $CaPd_3O_4$. However, even up to x = 0.20, the material remains semiconducting with a negative $d\rho/dT$, though the resistivity values are near identical to

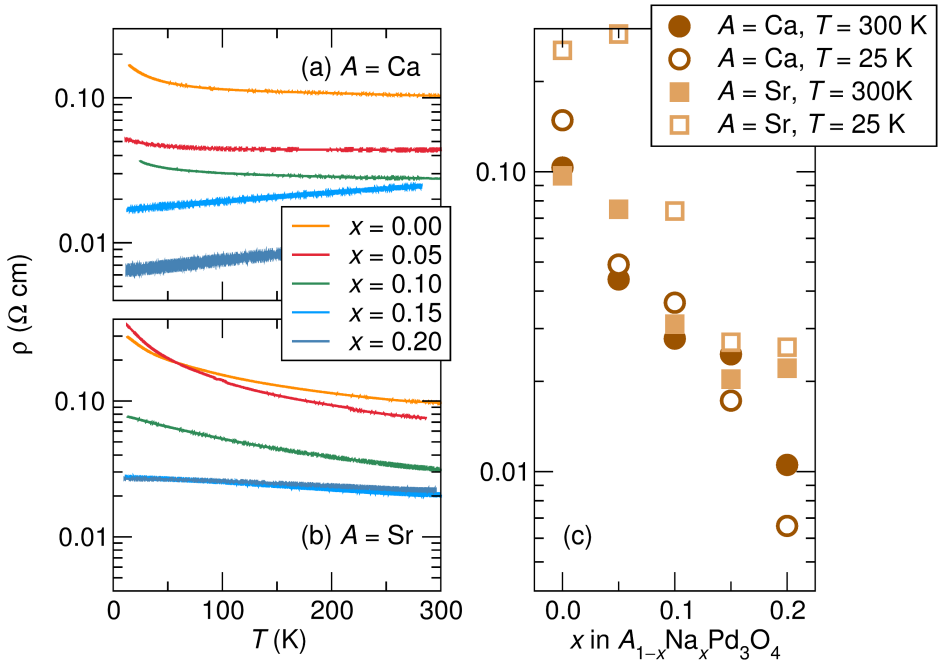

Figure 4: Resistivities of APd_3O_4 (A = Ca, Sr) with Na doping. $CaPd_3O_4$ undergoes an insulator-to-metal transition above $x = 0.10$ as seen through the decrease in resistivity with temperature at these levels. Despite similar room temperature resistivity values, $SrPd_3O_4$ does not undergo an insulator-to-metal transition even up to $x = 0.20$.

those reported by Taniguchi and co-workers.[18] This result is surprising as both materials were prepared and processed identically and from the lattice parameter changes appear to be incorporating the Na dopants up to 20 mol %.

To explore the differing electronic behavior in these compounds, DFT calculations were carried out to investigate any differences in the electronic structure. The density of states (DOS) for both of the pristine materials are shown in Figure 5. It is important to note that the DOS calculations were carried out using a hybrid functional in order to obtain a more accurate band gap value. The HSE calculations predict very small, nearly identical bandgaps of 0.25 eV for $CaPd_3O_4$ and 0.22 eV for $SrPd_3O_4$. Both compounds show significant Pd-d states just below the Fermi level. The DOS for both compounds possess similar features both below and above the Fermi level, and the band structures for both compounds are almost indistinguishable near the Fermi level. The extreme similarities in the electronic structures of these compounds implies that the differences in the onset of

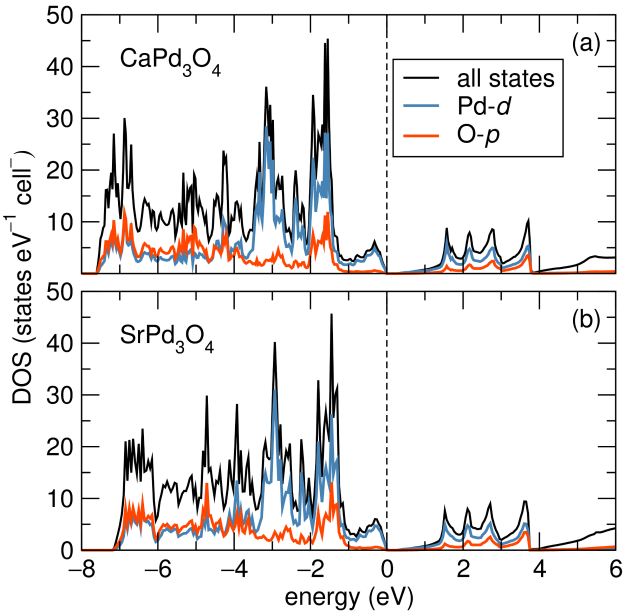

Figure 5: Density of states calculated using a hybrid functional for (a) $CaPd_3O_4$ and (b) $SrPd_3O_4$. The calculated bandgaps are 0.25 eV and 0.22 eV, respectively.

the insulator-to-metal transition are not due to any fundamental differences in the physics of the materials, but may be due to deviations in the local structure imparted through hole-doping.

Deviations from Average Structure: Structural Heterogeneities

Close inspection of the synchrotron diffraction data reveals that the nominal $Ca_{0.80}Na_{0.20}Pd_3O_4$ and $Sr_{0.80}Na_{0.20}Pd_3O_4$ samples have peak tails to higher Q on all Bragg peaks, highlighted in the (enlarged) difference curves presented in Figure 6. The tails are more pronounced in $Sr_{0.80}Na_{0.20}Pd_3O_4$. For both the Ca and Sr compounds substituted with only 5 mol % Na, the peaks appear symmetric and the difference curves do not reveal any features. The tails in the highly substituted samples suggest a deviation from the average crystallographic structure. This may be attributed to either a gradient or clustering of the Na dopants as the dopant concentration increases, as a uniform distribution of dopant ions should produce symmetric peaks with a corresponding shift in the lattice parameters.

Two different models were applied to better capture the peak tails in the 20 % substi-

tuted samples. To simulate a concentration gradient of Na dopants across the material, a model was created with 8 $Pm\bar{3}n$ phases with the lattice parameter and Na occupancy shifted by a constant amount between each phase. To simulate Na clustering, the second model was constructed of 2 phases where the Na concentration, lattice parameter, and size/strain contributions to the peak shapes were allowed to refine independently. These methods have been used in many material systems to examine phase separation and structural heterogeneity.[38,39] Figure 7 illustrates the fit of each model to the main reflection (021) of $Sr_{0.80}Na_{0.20}Pd_3O_4$. The total Na occupancy was not fixed in either of the models and refined to between 12 % and 16 % total occupancy. While both models are able to capture the peak tails, there is no substantial difference between the two, and the nature of the Na substitution is still unclear from analysis of the diffraction data.

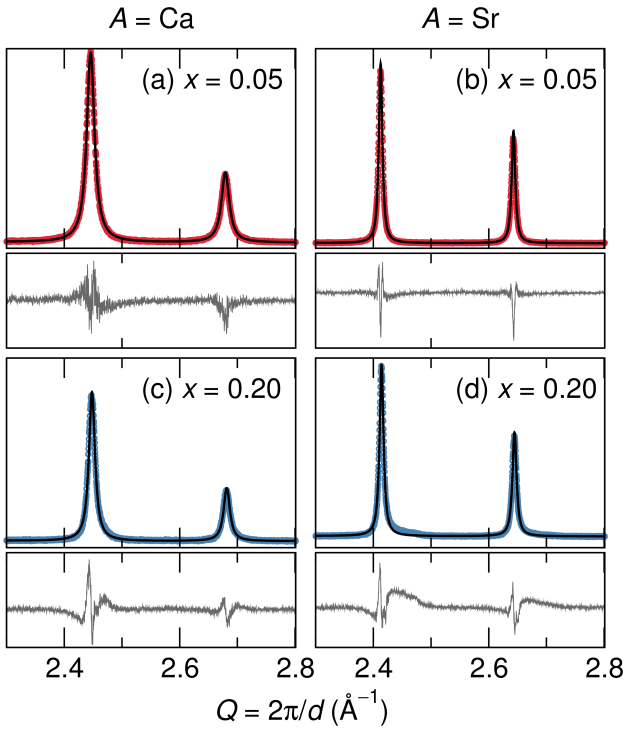

Figure 6: Diffraction patterns and Rietveld fits for the 5% Na-substituted (a) $CaPd_3O_4$ and (b) $SrPd_3O_4$ and (c,d) 20 % Na-substituted materials.While the 5 % substituted compounds have symmetric peak shapes, the peaks of the 20 % Na-substituted compounds have a tail to higher Q. This is clearly evident in the difference curves (enlarged for clarity) which possess a broad feature after every peak.

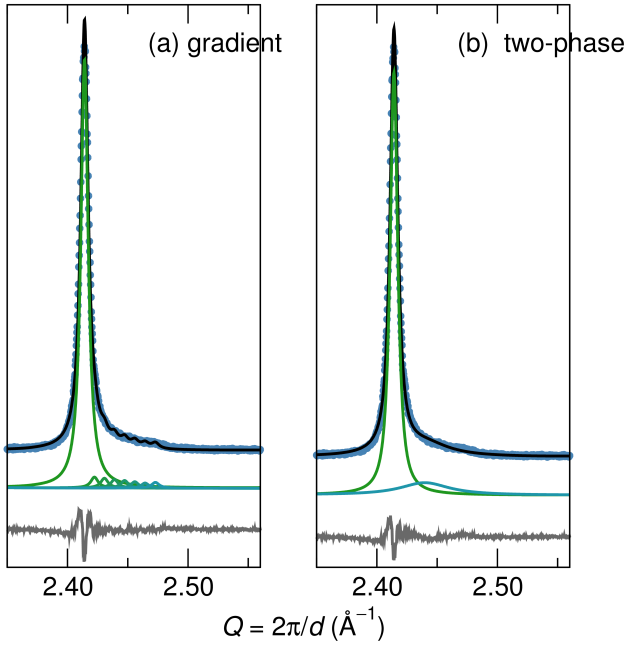

Figure 7: Fits of the primary (021) reflections of nominal $Sr_{0.80}Na_{0.20}Pd_3O_4$ using (a) an Na-gradient model and (b) a 2-phase Na-cluster model result in a similar quality fit.

The peak tails in synchrotron X-ray diffraction data of the highly substituted samples prompt a close study of the local structure in these materials in order to both explore the nature of the insulator-to-metal transition and to explain differences in the observed electronic properties. Neutron PDF data was utilized to investigate local deviations from the average crystallographic structure. Least squares fits of the PDFs are shown in Figure 8. The data was fit against the crystallographic structure with nominal site occupancies over a fit range of 1.5 Å to 5 Å. The results of the fits are given in Table 1.

By comparing the resulting fits against the average models, relative degrees of local disorder can be ascertained. As demonstrated by the goodness of fit parameters, R_w, (Table 1) the 5% substituted $CaPd_3O_4$ and $SrPd_3O_4$ are locally fit well with the average structure. Interestingly, the 20% substituted $SrPd_3O_4$ results in a poorer fit to the average model than the 20% substituted $CaPd_3O_4$, evidenced by a large increase in the resulting Rw value. This is indicative of a more locally disordered structure, and by examining the features of the PDF that are not being captured by the average model, the nature of the distortion may be qualitatively inferred. A significant peak shoulder occurring around 3 Å is present only in

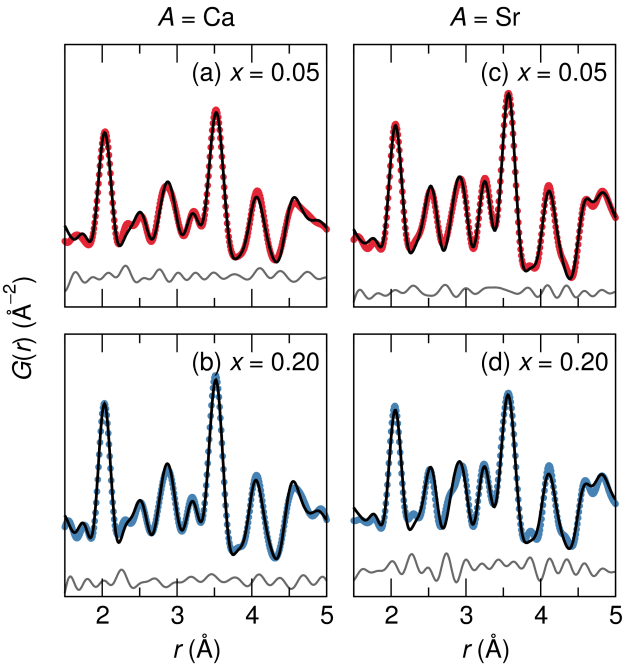

Figure 8: PDF fits against the crystallographic structures. Both of the lightly Na-substituted ($x = 0.05$) samples (a,c) and the highly Na-substituted ($x = 0.20$ b,d) $CaPd_3O_4$ are well fit with the average structure. The highly Na-subsituted $SrPd_3O_4$ is comparatively more poorly fit, indicating that the local environment is more disordered.

the highest substituted $SrPd_3O_4$. This correlation distance corresponds to the Pd–Pd and O–O interactions of proximal Pd square planar units. Thus, slight distortions of the Pd square planar network around Na dopants may be present, which is reasonable given the greater size difference between the Sr^{2+} and Na^{1+} ions. In addition to local distortions, any potential Na clustering may result in poorer fits to the local structure. A two phase fit including the possibility of a Na_2CO_3 impurity was attempted, as some amount of Na_2CO_3 was observed in solid state ^{23} Na NMR (see next section), though it did not improve the fit or capture the observed peak shoulder.

Deviations from Average Structure: Compositional Heterogeneities

In addition to PDF, solid-state ^{23}Na NMR was conducted to study the resolved local environment of the Na dopants in these materials. ^{23}Na is a spin 3/2 quadrupolar nucleus in 100% abundance, making it an attractive nucleus to study in the materials before and

Table 1: Results of fits of the neutron PDF data against the $Pm\bar{3}n$ models for $A_{1-x}Na_xPd_3O_4$ with $x = 0.05$ and 0.20 and A = Ca and Sr.

	A = Ca		A = Sr	
	$x = 0.05$	$x = 0.20$	$x = 0.05$	$x = 0.20$
a (Å)	5.759(4)	5.748(3)	5.829(3)	5.821(3)
A/Na U_{iso} (Å^2)	0.0078(18)	0.0077(15)	0.0040(7)	0.0028(7)
Pd U_{iso} (Å^2)	0.0042(6)	0.0034(4)	0.0034(4)	0.0044(4)
O U_{iso} (Å^2)	0.0070(8)	0.0064(6)	0.0055(5)	0.0058(6)
R_w (%)	12.7	11.0	9.0	17.7

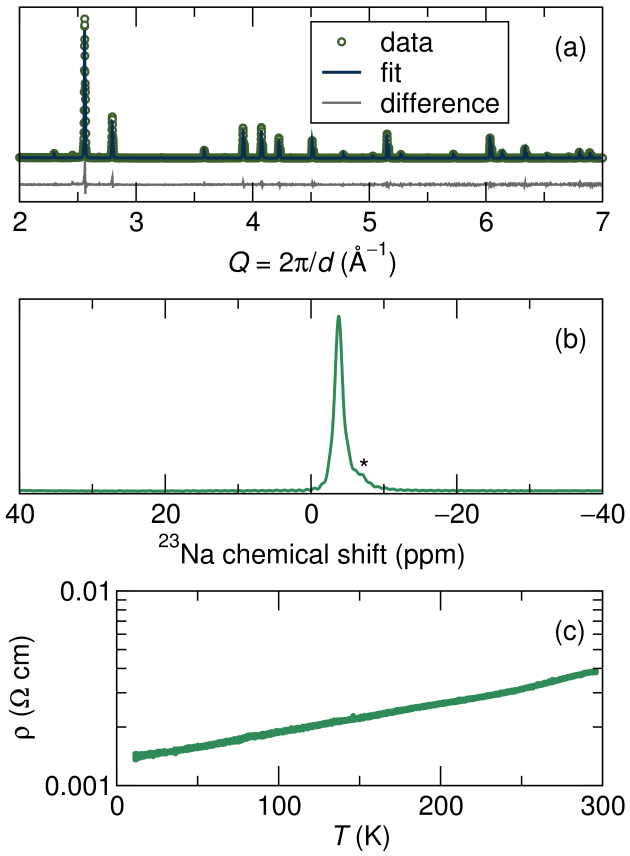

Figure 9: Results on the pure end-member ($x = 1$) compound $NaPd_3O_4$. (a) X-ray diffraction Rietveld refinement showing the phase pure nature of this composition. (b) ^{23}Na solid-state single pulse magic angle spinning NMR spectra (9.4 T, MAS at 8 kHz) showing a principle single peak corresponding to the single site in the crystal structure with a potential minor impurity on the right edge of the peak marked by (*). (c) Resistivity *vs.* temperature for a pressed pellet of $NaPd_3O_3$ showing the highly metallic nature of this hole-doped oxide.

after an insulator-to-metal transition as well as to examine differences between the Ca and Sr compounds. As a reference, we prepared metallic $NaPd_3O_4$, which possesses the same structure as $CaPd_3O_4$ and $SrPd_3O_4$ and can be thought of as a Na substitution level of x = 1.00. The structure of $NaPd_3O_4$ has been reported previously,[40,41] and reported electric properties are in agreement with our measurements.[17,26] A higher preparation temperature than was used for Na substitution in $CaPd_3O_4$ and $SrPd_3O_4$ was needed for phase purity. The different panels of Figure 9 summarize the results on this interesting metallic oxide. Figure 9(a) displays a Rietveld refinement of X-ray diffraction data of $NaPd_3O_4$ displaying a single cubic phase with a =5.638 Å. Figure 9(b) displays a dominant peak observed at -6 ppm, as is expected due to the single Na site in the structure. This peak is narrow due to the symmetric environment of the crystallographic site, despite the quadrupolar nature of the ^{23}Na nucleus. A small amount of a potential impurity marked by * in Figure 9 may also be present. Note that despite the metallic nature of the sample, established from the resistivity *vs.* temperature data shown in Figure 9(c), that the peak is not strongly Knight-shifted by the conduction electrons.[42] The ^{23}Na Knight shift can vary widely in magnitude and direction between various types of Na-substituted compounds,[43–45] but is generally expected to be small in a system like $NaPd_3O_4$ where the conduction states are derived from other atoms, namely Pd.

Figure 10 shows magic angle spinning (MAS) spectra of various Na substitution levels in $CaPd_3O_4$ and $SrPd_3O_4$. All of the spectra display two distinct Na environments which is surprising as the Na substitutes onto only one crystallographic site in these materials. A sharp peak centered at 7 ppm and a broad peak around -10 ppm are present at all levels of Na substitution in both series. The broad peak grows in intensity relative to the sharp peak with increasing Na substitution. A small amount of Na_2CO_3 was detected in the $SrPd_3O_4$ samples, denoted with a star in Figure 10. Based on the peak shape and chemical shift of the $NaPd_3O_4$ spectrum, we conclude the sharp peaks in the Ca and Sr compounds arise from Na in an undistorted environment, *i.e.* an isolated Na in the APd_3O_4 matrix. The

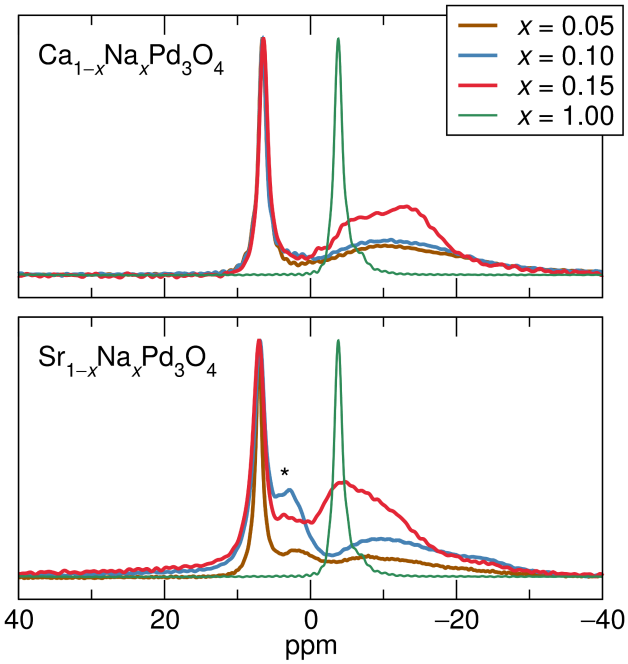

Figure 10: Single-pulse solid-state ^{23}Na MAS NMR spectra (9.4 T, MAS at 8 kHz) of Na-substituted $CaPd_3O_4$ and $SrPd_3O_4$. All of the Ca and Sr samples show 2 distinct Na environments represented by a sharp peak at 7 ppm and a broad signal centered around -10 ppm which grows relative to the sharp peak with increasing Na substitution. Metallic $NaPd_3O_4$ ($x = 1.00$) shows a single sharp peak at -6 ppm. The asterisk represents a small amount of Na_2CO_3 precursor.

insulating Ca/Sr matrix surrounding the isolated Na explains the differing chemical shifts in regards to the pure Na compound. The broad signal(s) appear at chemical shifts similar to the sharp peak of $NaPd_3O_4$, and thus we propose the origin of the broad peaks as arising from Na in metallic, Na-rich environments. The broadness may arise from a distribution in chemical shifts due to a distribution of the number of proximal Na atoms and/or a distorted Na coordination environment, leading to quadrupolar effects. In $SrPd_3O_4$, this peak is broader and more asymmetric in nature, further supporting a higher degree of disorder in comparison to the Ca sample at the same Na substitution level. Additionally, $SrPd_3O_4$ clearly shows a greater tendency for a clustering of the Na dopants at $x = 0.15$, as the broad peak begins to coalesce towards the $NaPd_3O_4$ ($x = 1.00$) peak. The $CaPd_3O_4$ samples do not show as clear a clustering at the Na substitution levels studied through NMR. The greater ionic size difference of Na and Sr most likely leads to the increased propensity for Na clustering. For both samples, the relative intensity of the broad peak grows with increasing Na concentration, suggesting a percolative insulator-to-metal transition mechanism. Even at small Na-substitution levels, there is evidence of metallic domains most likely arising from Na atoms in nearby proximity. However, the local disorder present in the Sr compounds limits the domain growth, thus preventing bulk metallicity.

^{23}Na NMR evidence suggests the formation of what appear to be metallic regions immediately upon Na substitution, despite bulk electrical transport suggesting that the samples remain in the insulating regime.This points to metallic and insulating regions in the sample that are phase-separated. This phenomena is well known in alkali-metal liquid NH_3 solutions, where the phase separation between more metallic, high alkali-content liquid from the insulating, less concentrated liquid can be physically observed, and has also been followed by NMR.[46] The phenomena of such microscopic phase separation was predicted by Mott,[47] who pointed out that the insulator and the metal must lie in separate minima of the free energy characteristic of first-order phase transitions. Similar local heterogeneity has been observed in Li-NMR of ^{7}Li-deintercalated $LiCoO_2$,[48] and in a study of Li-ordering

in $Li_{1-x}Sn_{2+}As_2$.[49]

In conclusion, Na has been substituted into both $CaPd_3O_4$ and $SrPd_3O_4$ under identical conditions and subtle differences in the local structure of these materials have been studied. Despite identical crystal and electronic structures, $CaPd_3O_4$ is more easily driven metallic with hole doping through Na substitution. Neutron pair distribution function data reveal $SrPd_3O_4$ is more locally disordered with high Na substitution. ^{23}Na NMR reveals an apparent percolative insulator-to-metal transition mechanism as metallic domains in the materials grow with increasing Na substitution. Increased disorder and a tendency for the Na to cluster when substituted into $SrPd_3O_4$ are believed to act against metallicity by limiting metallic domain growth. This work highlights the need for detailed local probes to elucidate differences in observed material properties that are not easily explained by average structure techniques such as diffraction.

Supporting Information

CIF files obtained from single-phase Rietveld refinement of synchrotron X-ray diffraction data of the nominal $Ca_{0.80}Na_{0.20}Pd_3O_4$ and $Sr_{0.80}Na_{0.20}Pd_3O_4$ compounds. As discussed in the main text, significant peak tails, particularly in the Sr sample, result in an underestimation of the Na occupancy.

Acknowledgement

This work was supported by the National Science Foundation through DMR-1403862. Helpful discussions with Raphäele Clément and Rahul Sangodkar are gratefully acknowledged. This manuscript has been co-authored by UT-Battelle, LLC under Contract No. DE-AC05-00OR22725 with the U.S. Department of Energy. The United States Government retains and the publisher, by accepting the article for publication, acknowledges that the

United States Government retains a non-exclusive, paid-up, irrevocable, worldwide license to publish or reproduce the published form of this manuscript, or allow others to do so, for United States Government purposes. The Department of Energy will provide public access to these results of federally sponsored research in accordance with the DOE Public Access Plan (http://energy.gov/downloads/doe-public-access-plan). The computational studies reported here made use of facilities supported by the Center for Scientific Computing at UCSB, supported by NSF MRSEC (DMR-1121053) and NSF CNS-0960316 and Hewlett Packard. The Materials Research Laboratory is a member of the NSF-supported Materials Research Facilities Network. Use of the Advanced Photon Source at Argonne National Laboratory was supported by the U. S. Department of Energy, Office of Science, Office of Basic Energy Sciences, under Contract No. DE-AC02-06CH11357. The use of the NOMAD instrument used resources at the Spallation Neutron Source, a DOE Office of Science User Facility operated by the Oak Ridge National Laboratory.

References

(1) Hensel, F.; Slocombe, D. R.; Edwards, P. P. On the Occurrence of Metallic Character in the Periodic Table of the Chemical Elements. *Phil. Trans. R. Soc. A* **2015**, *373*, 20140477.

(2) Imada, M.; Fujimori, A.; Tokura, Y. Metal-Insulator Transitions. *Rev. Mod. Phys.* **1998**, *70*, 1039–1263.

(3) Yang, Z.; Ko, C.; Ramanathan, S. Oxide Electronics Utilizing Ultrafast Metal-Insulator Transitions. *Annu. Rev. Mater. Res.* **2011**, *41*, 337–367.

(4) Snyder, G. J.; Toberer, E. S. Complex Thermoelectric Materials. *Nat. Mater.* **2008**, *7*, 105–114.

(5) Chu, C. W.; Deng, L. Z.; Lv, B. Hole-Doped Cuprate High Temperature Superconductors. *Phys. C* **2015**, *514*, 290–313.

(6) Fäth, M.; Freisem, S.; Menovsky, A. A.; Tomioka, Y.; Aarts, J.; Mydosh, J. A. Spatially Inhomogeneous Metal-Insulator Transition in Doped Manganites. *Science* **1999**, *285*, 1540–1542.

(7) Dagotto, E.; Hotta, T.; Moreo, A. Colossal Magnetoresistant Materials: The Key Role of Phase Separation. *Phys. Rep.* **2001**, *344*, 1–153.

(8) Baldini, M.; Muramatsu, T.; Sherafati, M.; Mao, H.-k.; Malavasi, L.; Postorino, P.; Satpathy, S.; Struzhkin, V. V. Origin of Colossal Magnetoresistance in $LaMnO_3$ Manganite. *Proc. Natl. Acad. Sci.* **2015**, *112*, 10869–10872.

(9) Raccah, P. M.; Goodenough, J. B. A Localized Electron to Collective Electron Transition in the System (La,Sr)CoO_3. *J. Appl. Phys.* **1968**, *39*, 1209.

(10) Wu, J.; Leighton, C. Glassy Ferromagnetism and Magnetic Phase Separation in $La_{1-x}Sr_xCoO_3$. *Phys. Rev. B* **2003**, *67*, 174408.

(11) Phelan, D.; Louca, D.; Kamazawa, K.; Lee, S.-H.; Ancona, S. N.; Rosenkranz, S.; Motome, Y.; Hundley, M. F.; Mitchell, J. F.; Moritomo, Y. Spin Incommensurability and Two Phase Competition in Cobaltites. *Phys. Rev. Lett.* **2006**, *97*, 235501.

(12) He, C.; El-Khatib, S.; Eisenberg, S.; Manno, M.; Lynn, J. W.; Zheng, H.; Mitchell, J. F.; Leighton, C. Transport Signatures of Percolation and Electronic Phase Homogeneity in $La_{1-x}Sr_xCoO_3$ Single Crystals. *Appl. Phys. Lett.* **2009**, *95*, 222511.

(13) Page, K.; Kolodiazhnyi, T.; Proffen, T.; Cheetham, A. K.; Seshadri, R. Local Structural Origins of the Distinct Electronic Properties of Nb-Substituted $SrTiO_3$ and $BaTiO_3$. *Phys. Rev. Lett.* **2008**, *101*, 205502.

(14) Uriu, R.; Shimada, D.; Tsuda, N. Metal to Insulator Transition in $Pd_{1-x}Li_xO$. *J. Phys. Soc. Japan* **1991**, *60*, 2479–2480.

(15) Ozawa, T. C.; Taniguchi, T.; Nagata, Y.; Noro, Y.; Naka, T.; Matsushita, A. Metal–Insulator Transition and Large Thermoelectric Power of a Layered Palladium Oxide: $PbPdO_2$. *J. Alloys Compd.* **2005**, *388*, 1–5.

(16) Ichikawa, S.; Terasaki, I. Metal-Insulator Transition in $Ca_{1-x}Li_xPd_3O_4$. *Phys. Rev. B* **2003**, *68*, 233101.

(17) Itoh, K.; Tsuda, N. Metal to Semiconductor Like Transition for Sintered $Ca_{1-x}Na_xPd_3O_4$. *Solid State Commun.* **1999**, *109*, 715–719.

(18) Taniguchi, T.; Nagata, Y.; Ozawa, T. C.; Sato, M.; Noro, Y.; Uchida, T.; Samata, H. Insulator-Metal Transition Induced in $Sr_{1-x}Na_xPd_3O_4$ for Small Na-Substitutions. *J. Alloys Compd.* **2004**, *373*, 67–72.

(19) Wang, X. L. Proposal for a New Class of Materials: Spin Gapless Semiconductors. *Phys. Rev. Lett.* **2008**, *100*, 156404.

(20) Hase, I.; Nishihara, Y. $CaPd_3O_4$ as an Excitonic Insulator. *Phys. Rev. B* **2000**, *62*, 13426–13429.

(21) Kurzman, J. A.; Miao, M.-S.; Seshadri, R. Hybrid Functional Electronic Structure of $PbPdO_2$, a Small-Gap Semiconductor. *J. Phys. Condens. Matter* **2011**, *23*, 465501.

(22) Savosta, M. M.; Novák, P. Two-Phase Character of Metallic Ferromagnetism in Manganites. *Phys. Rev. Lett.* **2001**, *87*, 137204.

(23) Kuhns, P. L.; Hoch, M. J. R.; Moulton, W. G.; Reyes, A. P.; Wu, J.; Leighton, C. Magnetic Phase Separation in $La_{1-x}Sr_xCoO_3$ by ^{59}Co Nuclear Magnetic Resonance. *Phys. Rev. Lett.* **2003**, *91*, 127202.

(24) Lamontagne, L. K.; Laurita, G.; Gaultois, M. W.; Knight, M.; Ghadbeigi, L.; Sparks, T. D.; Gruner, M. E.; Pentcheva, R.; Brown, C. M.; Seshadri, R. High Thermopower with Metallic Conductivity in p-Type Li-Substituted $PbPdO_2$. *Chem. Mater.* **2016**, *28*, 3367–3373.

(25) Muller, O.; Roy, R. *Platin. Gr. Met. Compd.*; Chapter 3, pp 28–38.

(26) Itoh, K.; Yano, Y.; Tsuda, N. Metal to Insulator Transition for $Ca_{1-x}Na_xPd_3O_4$. *J. Phys. Soc. Japan* **1999**, *68*, 3022–3026.

(27) Rietveld, H. M. A Profile Refinement Method for Nuclear and Magnetic Structures. *J. Appl. Crystallogr.* **1969**, *2*, 65–71.

(28) Coelho, A. A.; Evans, J.; Evans, I.; Kern, A.; Parsons, S. The TOPAS Symbolic Computation System. *Powder Diffr.* **2011**, *26*, S22–S25.

(29) *VESTA*: a Three-Dimensional Visualization System for Electronic and Structural Analysis. *J. Appl. Crystallogr.* **2008**, *41*, 653–658.

(30) Neuefeind, J.; Feygenson, M.; Carruth, J.; Hoffmann, R.; Chipley, K. K. The Nanoscale Ordered MAterials Diffractometer NOMAD at the Spallation Neutron Source SNS.

Nucl. Instruments Methods Phys. Res. Sect. B Beam Interact. with Mater. Atoms **2012**, *287*, 68–75.

(31) Billinge, C. L. F.; Juhas, P.; Liu, J. W.; Bryndin, D.; Božin, E. S.; Bloch, J.; Proffen, T.; L, S. J. PDFfit2 and PDFgui: Computer Programs for Studying Nanostructure in Crystals. *J. Phys. Condens. Matter* **2007**, *19*, 335219.

(32) Kresse, G.; Furthmüller, J. Efficiency of Ab-Initio Total Energy Calculations for Metals and Semiconductors Using a Plane-Wave Basis Set. *Comput. Mater. Sci.* **1996**, *6*, 15–50.

(33) Kresse, G.; Marsman, M.; Furthmüller, J. Vienna Ab-Initio Simulation Package: VASP the GUIDE. 2012.

(34) Kresse, G.; Joubert, D. From Ultrasoft Pseudopotentials to the Projector Augmented-Wave Method. *Phys. Rev. B* **1999**, *59*, 1758–1775.

(35) Perdew, J. P.; Burke, K.; Ernzerhof, M. Generalized Gradient Approximation Made Simple. *Phys. Rev. Lett.* **1996**, *77*, 3865–3868.

(36) Heyd, J.; Scuseria, G. E.; Ernzerhof, M. Hybrid Functionals Based on a Screened Coulomb Potential. *J. Chem. Phys.* **2003**, *118*.

(37) Shannon, R. D. Revised Effective Ionic Radii and Systematic Studies of Interatomic Distances in Halides and Chalcogenides. *Acta Crystallogr. Sect. A* **1976**, *32*, 751–767.

(38) Kaveh, S.; Tremblay, C. P.; Norhashim, N.; Curry, R. J.; Cheetham, A. K. Phase Separation in Garnet Solid Solutions and its Effect on Optical Properties. *Adv. Mater.* **2013**, *25*, 6448–6452.

(39) Doulgas, J. E.; Chater, P. A.; Brown, C. M.; Pollock, T. M.; Seshadri, R. Nanoscale Structural Heterogeneity in Ni-Rich Half-Heusler TiNiSn. *J. Appl. Phys.* **2014**, *116*, 163514.

(40) Scheer, J. J.; Arkel, A. E. V.; Heyding, R. D. Oxide Complexes Formed in the Systems Platinum Metals: Alkali Carbonates: Oxygen. *Can. J. Chem.* **1955**, *33*, 683–686.

(41) Panin, R. V.; Khasanova, N. R.; Abakumov, A. M.; Antipov, E. V.; Tendeloo, G. V.; Schnelle, W. Synthesis and Crystal Structure of the Palladium Oxides $NaPd_3O_4$, Na_2PdO_3 and $K_3Pd_2O_4$. *J. Solid State Chem.* **2007**, *180*, 1566–1574.

(42) Knight, W. D. Nuclear Magnetic Resonance Shift in Metals. *Phys. Rev.* **1949**, *76*, 1259–1260.

(43) Tunstall, D. P.; Ramage, W. A High-Pressure NMR Study of Sodium Tungsten Bronze: Na_xWO_3. *J. Phys. C Solid State Phys.* **1980**, *13*, 725.

(44) Riccó, M.; Fumera, G.; Shiroka, T.; Ligabue, O.; Bucci, C.; Bolzoni, F. Metal-to-Insulator Evolution in $(NH_3)_xNaK_2C_{60}$: An NMR study. *Phys. Rev. B* **2003**, *68*, 35102.

(45) Ramachandran, G. K.; Dong, J.; Sankey, O. F.; McMillan, P. F. $^{23}\mathrm{Na}$ and $^{29}\mathrm{Si}$ NMR Knight Shifts in the Silicon Clathrate $\mathrm{Na_{16}Cs_8Si_{136}}$. *Phys. Rev. B* **2000**, *63*, 33102.

(46) Lodge, M. T. J. H.; Cullen, P.; Rees, N. H.; Spencer, N.; Maeda, K.; Harmer, J. R.; Jones, M. O.; Edwards, P. P. Multielement NMR Studies of the Liquid–Liquid Phase Separation and the Metal-to-Nonmetal Transition in Fluid Lithium–and Sodium–Ammonia Solutions. *J. Phys. Chem. B* **2013**, *117*, 13322–13334.

(47) Mott, N. F. The Transition to the Metallic State. *Philos. Mag.* **1961**, *6*, 287–309.

(48) Ménétrier, M.; Saadoune, I.; Levasseur, S.; Delmas, C. The Insulator-Metal Transition Upon Lithium Deintercalation from $LiCoO_2$: Electronic Properties and ^{7}Li NMR Study. *J. Mater. Chem.* **1999**, *9*, 1135–1140.

(49) Lee, K.; Kaseman, D.; Sen, S.; Hung, I.; Gan, Z.; Gerke, B.; Pöttgen, R.; Feygenson, M.; Neuefeind, J.; Lebedev, O. I.; Kovnir, K. Intricate Short-Range Ordering and

Strongly Anisotropic Transport Properties of $Li_{1-x}Sn_{2+x}As_2$. *J. Am. Chem. Soc.* **2015**, *137*, 3622–3630.

For Table of Contents Only

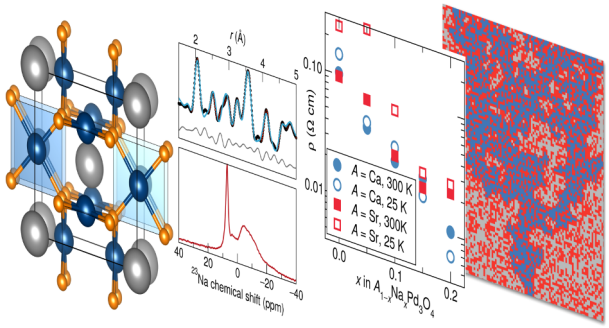

A number of different local and bulk probes of structure and composition have allowed sodium for alkaline-earth metal substitution and concomitant hole-doping of two complex palladium oxide systems to be studied, unravelling the role of structural and compositional heterogeneities in determining the electronic properties of the two distinct systems.